Fourier-transformed infrared spectroscopy study of the ancient ivory tusks from the Sanxingdui site

Xiaoguang Li[1]*, Chong Wang[2]*, Yu Zhang[3,4], Ruojing Zhang[5], Sifan Li[2], Qing Xiao[2] and Wen Su[1]

[1]State Key Laboratory of Lithospheric Evolution, Institute of Geology and Geophysics, Chinese Academy of Sciences, Beijing, China, [2]Sichuan Provincial Institute of Cultural Relics and Archaeology, Chengdu, China, [3]Key Laboratory of Cenozoic Geology and Environment, Institute of Geology and Geophysics, Chinese Academy of Sciences, Beijing, China, [4]College of Earth and Planetary Sciences, University of Chinese Academy of Sciences, Beijing, China, [5]School of Archaeology and Museology, Sichuan University, Chengdu, Sichuan, China

The archeological site at Sanxingdui preserves a considerable amount of ancient ivory tusks in its artifact pits, and accurately and quantitatively analyzing the original chemical signatures of these ivory tusks is a critical step in interpreting their buried history. In this study, 123 unearthed ivory tusks were characterized using Fourier-transformed infrared spectroscopy (FTIR), and seven *in situ* heating experiments were conducted. The hydroxylapatite crystallinity and carbonate concentration were quantitatively determined in line with the absorbance peak intensities of the corresponding bands. The average values of splitting factor (SF), type B carbonate/type A carbonate ratio (BC/AC), carbonate/phosphate ratio (C/P), type B carbonate/phosphate ratio (BPI), type A carbonate/phosphate ratio (API), and water−amide on the phosphate index (WAMPI) were calculated to be 3.84, 0.98, 0.12, 0.37, 0.38, and 0.11, respectively. The ratios of the $1,416\ cm^{-1}$–$1,454\ cm^{-1}$ carbonate bands of the ivory tusks were used to quantitatively estimate the different types of carbonate content in the ivory tusks. Heating experiments were designed to simulate the effect of heat on the hydroxylapatite structures. We suggest that the SF and the C/P indices can serve as distinctive preservation indices of ancient ivory tusks as well as the BC/AC index and hydroxyl types.

KEYWORDS

hydroxylapatite, FTIR, ivory tusk, carbonate, crystallinity

1 Introduction

The Sanxingdui site, which is located in Sichuan Province, China, has fascinated archeologists due to its unparalleled archeological treasure trove of artifact pits (Shi, 2005; Xu, 2008; Chi, 2013; Ge and Linduff, 2015; Yang and Xu, 2022). Buried underground for more than 3,000 years, the ancient ivory tusks found at the site deserve careful protection and research (Zheng et al., 2013; Lai, 2015). As a physical carrier of an ancient civilization,

these artifacts need to be studied in detail using modern testing technology (Flad, 2012). Ivory tusk is a type of mineral composite consisting of hydroxylapatite (HA) and collagen (Locke, 2008; Jantou-Morris et al., 2010). The primary inorganic mineral component of ivory tusks is HA, with a stoichiometric composition of $Ca_5(PO_4)_{3-x}(CO_3)_x(F, Cl, OH)_y(CO_3)_{1-y}$ (Jantou-Morris et al., 2010; Virág, 2012), in which carbonate from the HA reflect the composition of the living environment of the elephant. As a mineral that connects the biosphere with the abiotic sphere, its composition and mineral structure can provide a variety of research information in a wide range of chemical and biological sciences. Ivory tusks store biological information from the time when the elephant they came from was alive. Hence, they can be used to extract significant information, such as the elephant species and the elephant's living environment (Banerjee et al., 2008).

To accurately identify their original chemical signature, we need to evaluate the preservation state of the mineral structure and chemical compositions of the ivory tusks as they were exposed to burial and weathering (Müller and Reiche, 2011). The HA in ivory tusks is always a poorly crystalline nonstoichiometric mineral composed of nanoparticles or microparticles. Specifically, the carbonate, hydroxyl, and collagen matrix of the HA induces disorder in the mineral lattice and thus limits its degree of crystallinity (Lebon et al., 2008). Organic matter decomposes during burial, leaving behind an inorganic mineral skeleton, and post-burial diagenesis induced by high temperatures or collagen decomposition typically causes the recrystallization of HA (Surovell and Stiner, 2001). The structure of the ivory tusks may also be affected by high temperatures incurred by climatic events or artificial fires (Lebon et al., 2008; Yan et al., 2022). Archeological studies have shown that high temperatures and weathering can cause the degradation of collagen and increase mineral crystallinity (Bortolaso, 2008; Gong et al., 2019).

Hence, assessing the preservation state of ivory tusks has become the primary focus of research. Fourier-transformed infrared (FTIR) spectroscopy is often used to determine the mineral composition and structure of a substance (Edwards and Farwell, 1995; Paris et al., 2005). The preservation indices for bone and dentin have been established using FTIR absorption band ratios (Thompson et al., 2009; Shaltout et al., 2011; Thompson et al., 2011; France et al., 2020). For example, the percentage of carbonation attributed to the stretching vibrations of carbonate and phosphate can be analyzed with the A1420/A565 ratio. IR spectroscopy can provide quali-quantitative results regarding the types of carbonate substitutions in HA (Wright and Schwarcz, 1996; Krajewski et al., 2005; Thompson et al., 2009; Hammerli et al., 2021). Because it is easy to use and does not destroy the subject of its analysis, FTIR has become an increasingly widely used method for determining the bioapatite preservation state in archeological research. For archeological burnt bone samples, the degree of bone heating can be evaluated

by the sum of the fourth-derivative spectra of the peak positions at 961, 1,022, and 1,061 cm^{-1} (Lebon et al., 2008). However, diagenetic processes will have partially removed the heating signal by alteration of the peak position, even for HA in bones (Lebon et al., 2008), and an evaluation system based on modern and archeological bones (Lebon et al., 2008; Lebon et al., 2010; Ellingham et al., 2016) will not function well for ancient ivory tusks. Furthermore, the sample concentrations and wavenumber positions produced by curve fitting can be personalized depending on the data analysis. As a result, lateral contrast has become a troublesome issue. Due to the small size of apatite and the presence of micropores in ancient ivory tusks, the absorption of a large amount of molecular water can occur, and previous tests have not been able to distinguish the hydroxyl structures with accuracy.

In this study, we present the preservation state of ancient ivory tusk fragments from the Sanxingdui site. *In situ* heating experiments were performed, and the hydroxyl vibration behavior upon heating was analyzed. The crystallinity, carbonate content, and temperature effect of the ivory tusks were then evaluated using FTIR.

2 Experimental method

2.1 Samples

In this study, 123 ancient ivory tusks, labeled s8–s210, were unearthed at the Sanxingdui site.

2.2 Instrumentation and operating conditions

The FTIR spectra were collected using a Bruker Vertex 70V spectrometer. The samples were prepared using potassium bromide (KBr) pellets with ca. 2% by mass of the sample in KBr at the Institute of Geology and Geophysics, Chinese Academy of Science (IGGCAS). The FTIR spectra were recorded in 64 scans between 400 and 4,000 cm^{-1} with a resolution of 4 cm^{-1}. A Hyperion 2000 IR microscope with a mercury cadmium telluride (MCT) detector cooled with liquid nitrogen connected to the Bruker Vertex 70V spectrometer was used to obtain the microscopy IR spectra for the *in situ* heating experiments. All spectra from the heating experiments were obtained in a spectral range from 4,000 to 650 cm^{-1} using 64 scans at a resolution of 4 cm^{-1}.

For the heating experiments, the effect of temperature on the FTIR spectra of the samples was investigated using a Linkam TS 1400XY heating stage (Linkam Scientific Instruments) at the IGGCAS. *In situ* heating experiments were conducted from room temperature to 800°C with 50°C intervals. The temperature accuracy and stability were ±1°C. Nitrogen was circulated at a
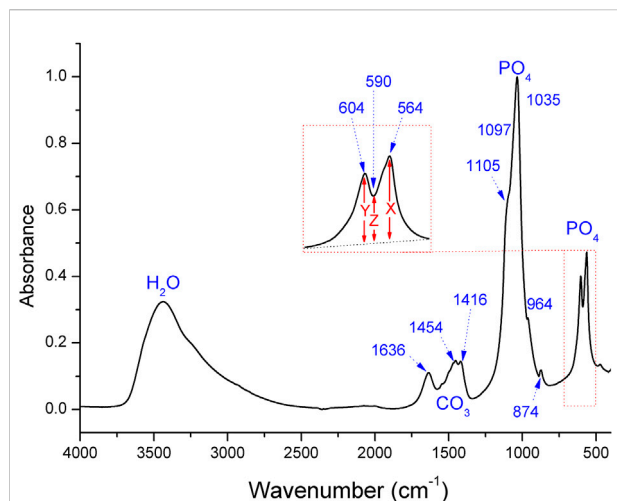
FIGURE 1
FTIR spectra for the s186 ancient ivory tusk, where the chemical groups and absorption bands are indicated. X, Y, and Z denote the heights of the peaks and the valleys. The numbers in parentheses represent the approximate positions of the apparent bands.

flow rate of approximately 60 ml/min through the furnace during the test. The original ivory tusk powder samples were placed on a sapphire disc within the temperature stage. The upper window of the temperature stage was made of quartz. Each test was conducted after 5 min of temperature retention.

2.3 Data processing

The raw data were baseline-corrected using the "concave rubberband" algorithm (10 iterations and 64 baseline points) using OPUS 7.5 software from Bruker in order to precisely measure the absorbance.

The infrared splitting factor (SF), also known as the phosphate crystallinity index or the crystallinity index, was calculated using the absorption bands labeled in Figure 1. The splitting function was measured as the heights of the phosphate double peaks divided by the heights of the troughs between them. We calculated the SF by measuring the relative lengths of the X (564–565 cm^{-1} peak), Y (604–605 cm^{-1} peak), and Z (the height of the valley between the X and Y peaks) of the 123 samples (Thompson et al., 2009, 2011; France et al., 2020).

The carbonate/phosphate ratio (C/P) was calculated based on the 1,416 cm^{-1} peak divided by the peak at 1,035 cm^{-1} (France et al., 2020).

The amount of type B carbonate to phosphate (BPI) ratio was calculated by dividing the intensity of the 1,416 cm^{-1} band by the intensity of the 604 cm^{-1} band. Similarly, the type A carbonate to phosphate (API) ratio was obtained by dividing the band intensity at 1,454 cm^{-1} by the intensity of the 604 cm^{-1} band (Sponheimer and Lee-Thorp, 1999; France et al., 2020).

The type B carbonate/type A carbonate ratio (BC/AC) was determined by dividing the band intensity of the peak at 1,416 cm^{-1} (type B) by the peak at 1,454 cm^{-1} (type A) (Wright and Schwarcz, 1996; Thompson et al., 2009; Thompson et al., 2011).

Water–amide on the phosphate index (WAMPI) was calculated by dividing the intensity of the band at 1,630–1,650 cm^{-1} by the intensity of the phosphate band at 604–605 cm^{-1} (Snoeck and Pellegrini, 2015; Roberts et al., 2020; Fernandes et al., 2022).

3 Results

3.1 Relationships between the Fourier-transformed infrared spectroscopy indices

By way of example, Figure 1 shows the FTIR spectra of the s186 ancient ivory obtained from the Sanxingdui site. In general, the FTIR spectra obtained from the KBr pellets indicated the presence of phosphate, hydroxyl, and carbonate ions in all of the ivory tusks, while the characteristic C-H absorption bands in the organic parts were absent in all of the samples. The remaining molecular water in these samples was predominant.
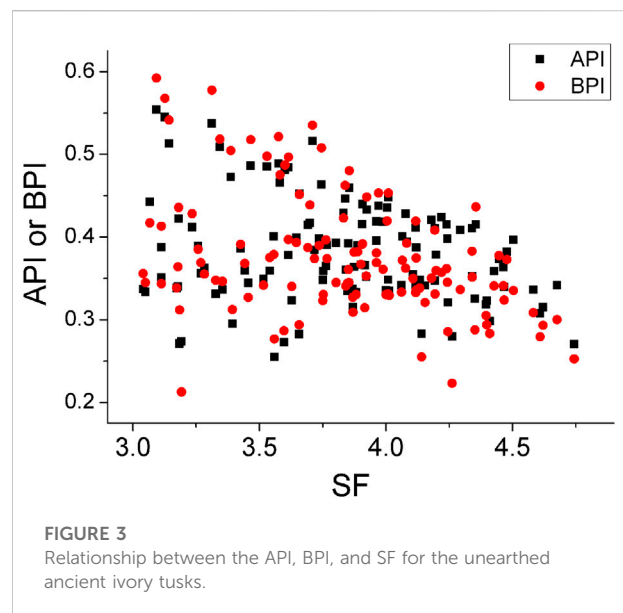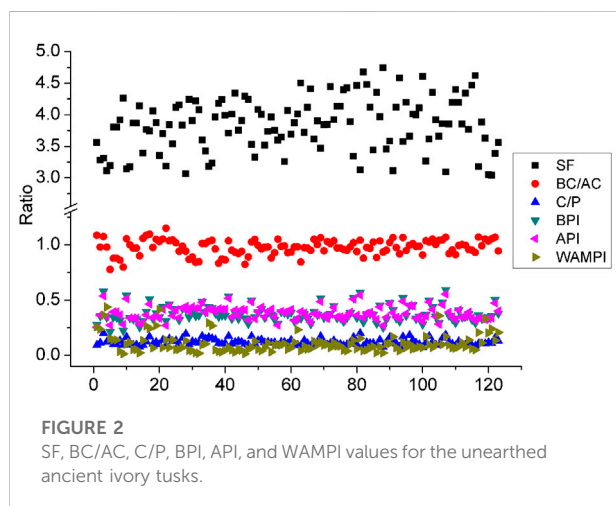
As shown in the spectra, the broadband at approximately 3,440 cm^{-1} was assigned to molecular water (Figure 1) that was adsorbed on the surfaces or micropores of HA (Ooi et al., 2007), while the 1,633–1,650 cm^{-1} peak was thought to correspond to the vibrations of the N-H or O-H bonds (Botha et al., 2004; Pekounov and Petrov, 2008). The absorption bands of carbonate were observed as doublet peaks at 1,452–1,458 cm^{-1} and 1,411–1,416 cm^{-1} (Yoder et al., 2018). The v2 mode of the carbonate band was at approximately 875–870 cm^{-1} (Fleet, 2009; Madupalli et al., 2017). The strong absorption bands at 1,105 and 1,035 cm^{-1} were assigned to the phosphate ions, and the peak at 964 cm^{-1} referred to the stretching mode of the P–O bond (Ooi et al., 2007). The FTIR spectra of all of the samples showed pronounced peaks at 564 and 604 cm^{-1} due to the presence of the phosphate group (Wright and Schwarcz, 1996; Miller et al., 2001; Grunenwald et al., 2014). Table 1 presents the band regions of these bands for all of the samples, with similar peak positions as in previous studies (Farlay et al., 2010; Roche et al., 2010; Yoder et al., 2012; Mandair and Morris, 2015).

As for the presently studied ivory tusks, Figure 2 shows a comparison of the indices (SF, BC/AC, C/P, BPI, API, and WAMPI) of all of the 123 samples measured in the transmission mode, with value ranges of [3.0, 4.7], [0.77, 1.1], [0.07, 0.20], [0.59, 0.21], [0.55, 0.25], and [0.02, 0.44], respectively. The average values of SF, BC/AC, C/P, BPI, API, and WAMPI were 3.84, 0.98, 0.12, 0.37, 0.38, and 0.11, respectively. Crystallinity has been of interest to archeologists as a rough quantitative measure or index of the extent of ivory tusk preservation and diagenetic alterations (France et al., 2020;

TABLE 1 Positions and assignments of the FTIR bands for all of the analyzed samples.

Position (cm⁻¹)	Assignments	Intensity	Chemical groups
3,568	O-H stretching of hydroxyl groups	w	OH
3,440	O-H stretching of molecular water (v1 and v3)	m	H_2O
1,633–1,650	N-H or O-H bond	w	NH; OH; CO
1,543–1,547	Carbonate asymmetric stretching (v3)	w	C-O (type A)
1,502	Carbonate stretching n3	w	C-O
1,452–1,458	Carbonate asymmetric stretching (v3)	m	C-O (type A)
1,411–1,416	Carbonate asymmetric stretching (v3)	m	C-O (type B)
1,097	Phosphate stretching (v3)	s	P-O
1,035	Phosphate asymmetric stretching (v3)	vs	P-O
964	Phosphate symmetric stretching (v1)	vs	P-O
880–878	Carbonate bending (v2)	w	C-O (type A)
874	Carbonate bending (v2)	w	C-O (type B)
604	Phosphate bending (v4)	m	P-O
564	Phosphate bending (v4)	m	P-O
473	Phosphate bending (v2)	w	P-O

w, weak; m, medium; s, strong; vs, very strong.

FIGURE 2
SF, BC/AC, C/P, BPI, API, and WAMPI values for the unearthed ancient ivory tusks.

FIGURE 3
Relationship between the API, BPI, and SF for the unearthed ancient ivory tusks.

Fernandes et al., 2022). The SF, indicating the degree of separation of the 564–565 cm⁻¹ and the 604–605 cm⁻¹ band, has typically been applied in the evaluation of the mineral crystallinity of HA (Weiner and Bar-Yosef, 1990). The SF, a measure of crystal order based on phosphates in HA, will increase after embedding (Lebon et al., 2008).

The hexagonal structure of the HA can accommodate carbonate ions in the c-axis structural channel where they will substitute hydroxyls (type A carbonate, $Ca_{10}(PO_4)_6[(OH)_{2-2x}(CO_3)_x]$) or phosphate groups (type B carbonate, $Ca_{10-x}[(PO4)_{6-x}(CO3)_x](OH)_{2-x}$) (Tacker, 2008). Typically, HA contains less than 10 wt.% carbonate ions (Featherstone et al., 1984; Krajewski et al., 2005). For the ivory in this assessment, carbonate was partially removed as recrystallization of HA

occurred (Figure 3). The C/P index, API, and BPI also correlated well, as shown in Figure 4. We could fit their relational equations as follows:

$$y = 1.8365x + 0.1622 \, (API) \tag{1}$$

$$y = 2.2332x + 0.1071 \, (BPI) \tag{2}$$

However, the API value was higher than the BPI value when the C/P index was less than 0.14, while the opposite situation occurred when the C/P index was larger than 0.14. The BC/AC and SF indices showed a weak negative correlation (Figure 5), whereas a linear relationship between the BC/AC and C/P indices
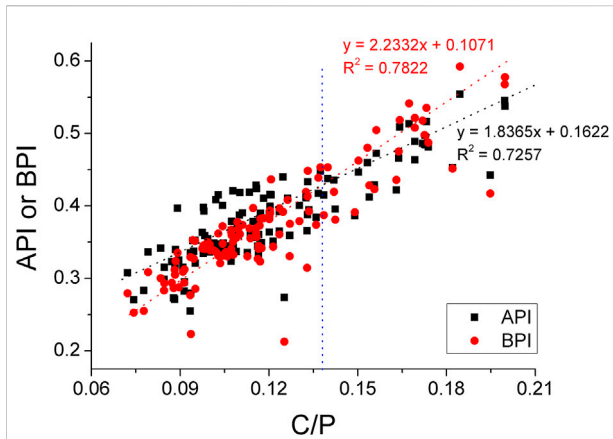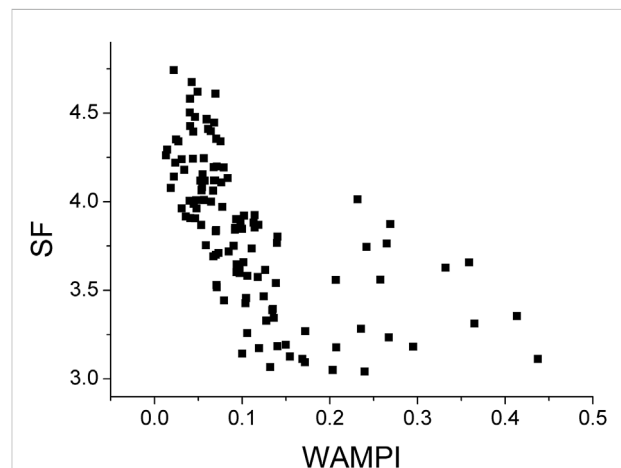
FIGURE 4
Relationship between the API, BPI, and C/P for the unearthed ancient ivory tusks.
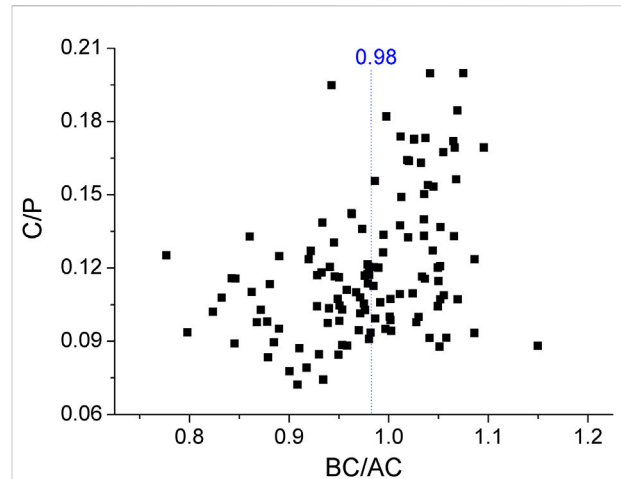
FIGURE 6
Scattergrams of the C/P plotted against the BC/AC.
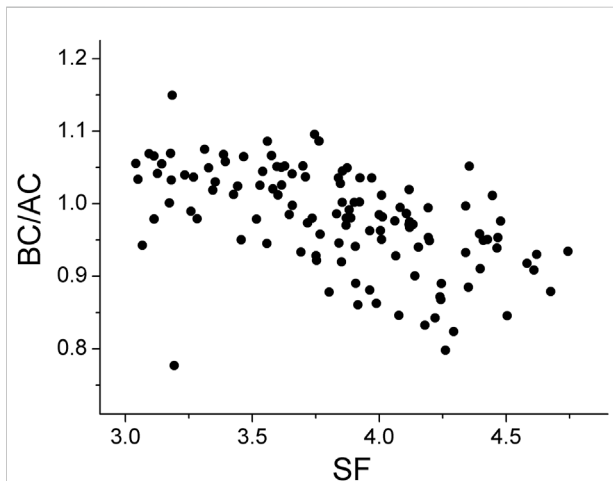
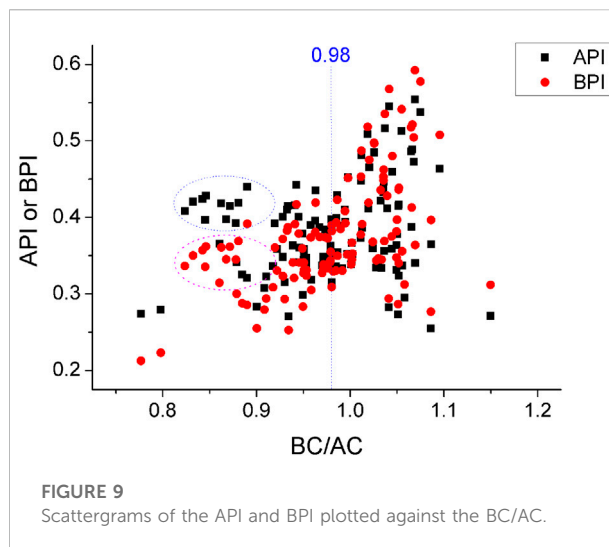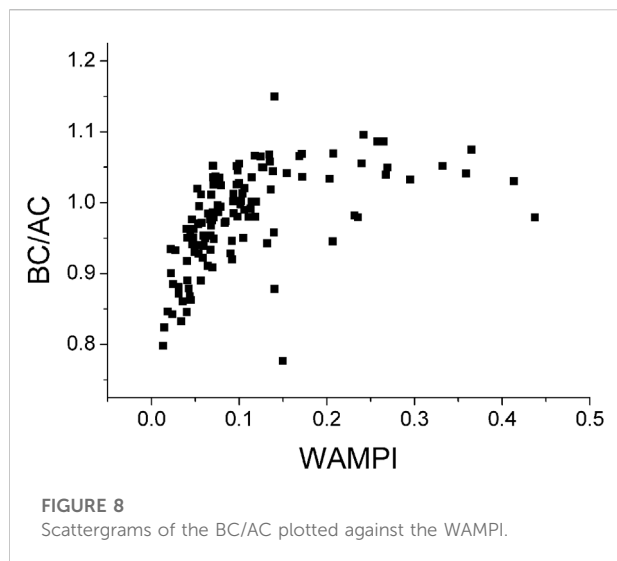
FIGURE 5
Scattergrams of the BC/AC plotted against the SF.

FIGURE 7
Scattergrams of the SF plotted against the WAMPI.

was minimally observed (Figure 6). For most studied ivory tusks, the WAMPI and SF have been negatively correlated (Figure 7), while the WAMPI and BC/AC have shown a positive correlation (Figure 8).

Although the BPI and API indices were correlated with one another (Figure 4), as shown in Figure 9, the BPI and API, which measure type B and type A carbonate, had a significantly different relationship with the BC/AC index. For the samples with a BC/AC value less than 0.98, the API value was usually larger than the BPI value (Figure 9). However, for the samples with higher BC/AC values, the BPI became dominant. Furthermore, the mass fraction of type B carbonate decreased with an increase in the SF value (Figures 3, 5).

3.2 Heating experiments

Figure 10 presents the FTIR spectra of the *in situ* heated unearthed ancient ivory tusks with increasing temperature. The broadband centered at approximately 3,400 cm^{-1} showed that the porous HA absorbed a significant amount of molecular water (Figure 10) (Meejoo et al., 2006; Madhavasarma et al., 2020). This broad and strong absorption peak of molecular water often overlapped the peak of the hydroxyl group in apatite, causing the hydroxyl peak to be unresolved between 25°C and 100°C (Figures 10A, B). The weak absorption peak located at 3,568 cm^{-1} became well-resolved only when the temperature was higher than 150°C (Shaltout et al., 2011; Yoder et al., 2012). The intensity of the molecular water stretching band also increased with the

FIGURE 8
Scattergrams of the BC/AC plotted against the WAMPI.

FIGURE 9
Scattergrams of the API and BPI plotted against the BC/AC.

cooling of temperature (data not shown), indicating reabsorption of the molecular water on the HA surface or internal channels.

As the temperature increased from 25°C to 800°C, the peak of the structural hydroxyl at 3,568 cm^{-1} gradually decreased in wavenumber with increasing temperature. The hydroxyl peak showed a wavenumber shift of 10 cm^{-1} between 25°C and 800°C, which was attributed to the thermal effect. For the s5 sample, however, the 3,543 cm^{-1} hydroxyl peak remained relatively stable because it was newly formed at about approximately 400°C (Rujitanapanich et al., 2014). For the s61 sample, the 3,543 cm^{-1} hydroxyl peak already existed before heating (Figures 10A), which possibly indicated that this sample was previously subjected to high temperatures (Figures 10, 11). The group of weak intensity bands in the 1,950–2,200 cm^{-1} region was derived from the overtones and combinations of the v3 and v1 PO_4^{3-} modes (Markovic et al., 2004; Ooi et al., 2007).

The "unheated HA" carbonate possessed 1,416 and 1,454 cm^{-1} peaks with nearly equal intensities (Thompson et al., 2009; Thompson et al., 2011; France et al., 2020). However, for the presently studied ivory tusks, the BC/AC dropped notably after the 800°C heating process (Figure 12). This meant that the type B carbonate decomposed when heated over 400°C, and this was also indicated by the emergence of the new hydroxyl peak (Figure 10B).

4 Discussion

4.1 The preservation state

Previous studies have made similar observations where recrystallization during burial may result in a more ordered crystal structure and higher SF values. It has been reported that well-preserved archeological bone has an upper SF value of 3.86 and a lower BC/AC value of 0.95 (France et al., 2020), and

these are similar to the average values obtained in this study. For the most studied bioapatite samples, the API and BPI ratio decreases slightly with increases in the SF (Lebon et al., 2008; Thompson et al., 2011; Pedrosa et al., 2020; Seredin et al., 2020). This was due to the loss of organic matter during burial. The use of the WAMPI values in an ivory tusk evaluation may fail to determine the small fraction of some well-preserved samples due to the influence of water. Approximately 48% of the studied samples showed SF values greater than 3.86, and 37% of the studied samples showed BC/AC values less than 0.95. This indicated a poor preservation level. In general, the SF and BC/AC index values showed that approximately 60% of the unearthed ivory tusks were well-preserved if the bone preservation indices were applied (France et al., 2020). In this manner, we obtained a threshold C/P value of 0.10 for well-preserved ivory tusks according to the C/P value range. However, the value range of the C/P index was small, and the calculation error possibly affected the evaluation results.

The BC/AC values showed a relative concentration of type B carbonate and type A carbonate, where type B carbonate accounted for approximately 50% of the total carbonate of the studied samples. The observed differences in the BPI and API indices were possibly due to the alternative thermal decomposition of type B carbonate with the emergence of Ca-OH. In the natural environment, the decomposition rate of type B carbonate is higher than that of type A carbonate; thus, the value of BC/AC decreased with organic loss. For this reason, a combined assessment of C/P and BC/AC indices could be applied to produce a reliable result when monitoring the preservation state of ancient ivory tusks.

4.2 Possible heating event

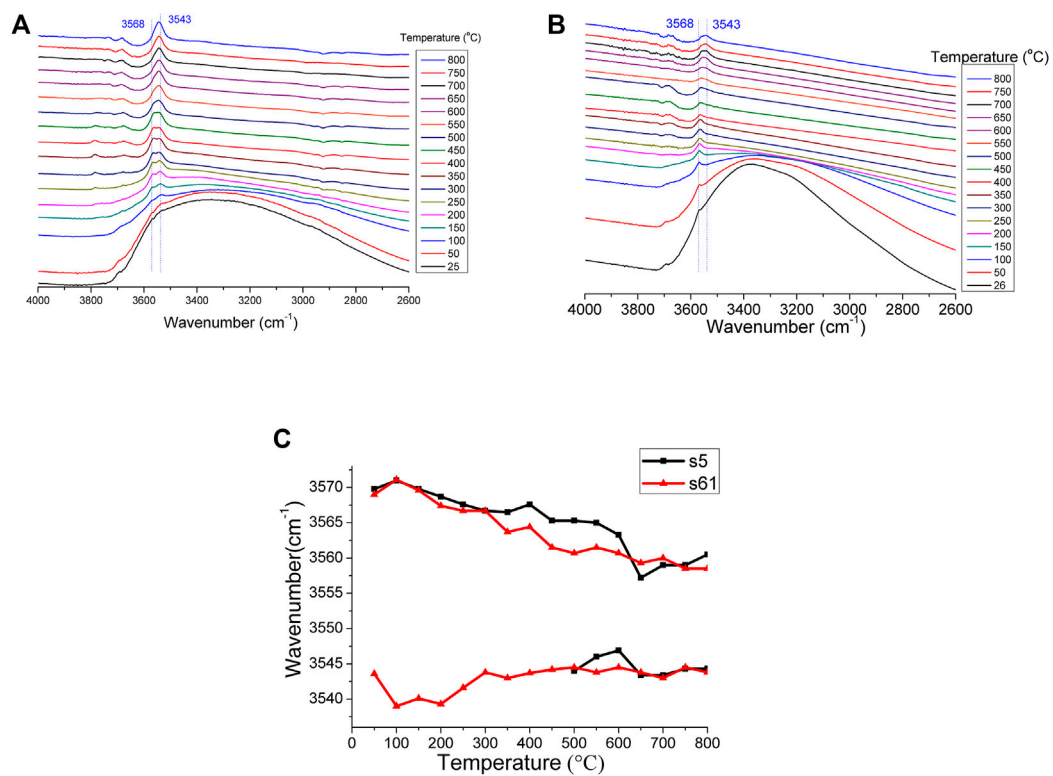The FTIR spectra of the unearthed ivory tusks measured at room temperature typically exhibit a broadband of molecular

FIGURE 10
IR spectral changes in the shape and position of hydroxyl absorption with temperature for **(A)** the s61 sample and **(B)** the s5 sample, and the **(C)** temperature dependence of the peak position of the hydroxyl of the s5 and s61 samples.
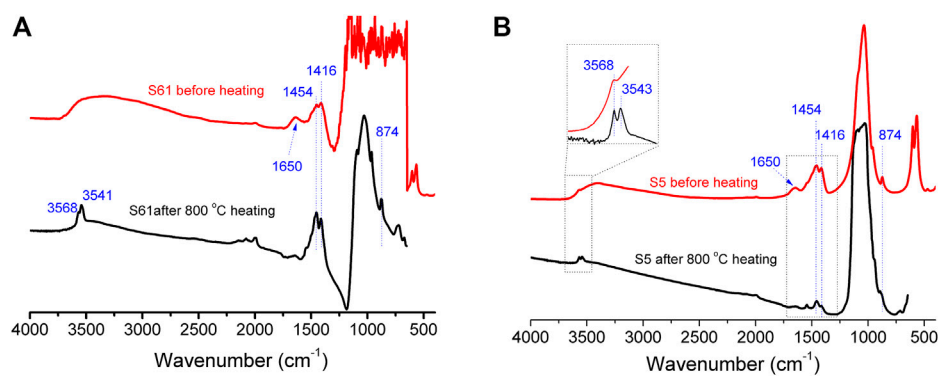
FIGURE 11
IR absorption spectra before and after 800°C heating of the **(A)** s61 sample and the **(B)** s5 sample.

water located in the cavities that are generated by the loss of original organic matter. The superimposition of the broad absorption band for molecular water onto the O-H peak at 3,568 cm^{-1} (Figure 10) possibly resulted in a misinterpretation of the FTIR peak. *In situ* heating FTIR can be applied as a valuable

tool to exclude this effect. Molecular water species exist in these ivory tusks but are not structurally bound in the apatite channel (Yoder et al., 2012). Molecular water would leave the HA crystal structure through the termination sites of the c-axes channels at temperatures above approximately 100°C. The decrease of the

FIGURE 12
Scattergrams of the BC/AC values before and after 800℃ heating of the s61, s107, s5, s96, s103, s179, and the s211 sample.
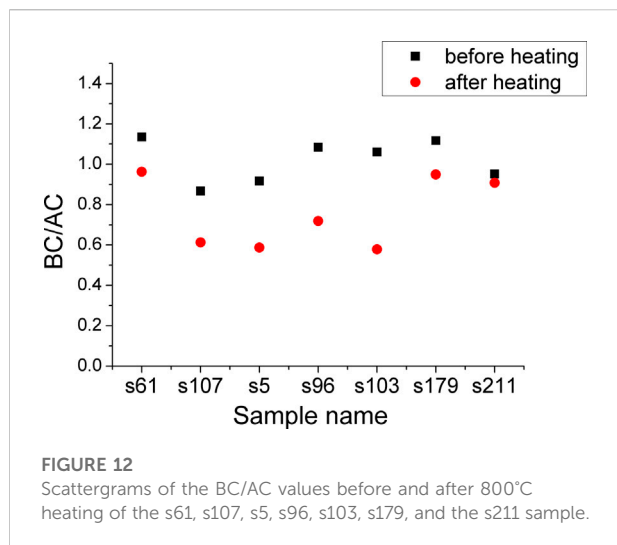
3,300–3,417 cm⁻¹ broadband between 25℃ and 200℃ primarily corresponded to the molecular water loss upon heating.

The bands at 3,568 cm⁻¹ represented the structural hydroxyl bands, while the new band at 3,543 cm⁻¹ indicated the formation of Ca-OH. We can make a speculation that decarbonization begins from approximately 400℃ through reactions 3–6 listed in this section, which is lower than that of the synthetic HA (Lafon et al., 2008; Tonsuaadu et al., 2012). This was possibly due to the porous structure and larger specific surface area resulting from the loss of organic matter that increased the reactivity of carbonate. According to an analysis of the peak intensity before and after the heating experiments, the carbonate composition of the analyzed ivory tusks was altered with a drop in the BC/AC index (Figure 12) (Munro et al., 2007). It was clear that the ν3 region of the type B carbonate had less FTIR intensity after heating, indicating the partial decomposition of carbonate to CO_2 through the following reactions:

$$CO_3^{2-} + H_2O = 2OH^- + CO_2 \tag{3}$$

$$CaCO_3 = CaO + CO_2 \tag{4}$$

$$CaO + H_2O = Ca(OH)_2 \tag{5}$$
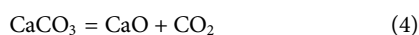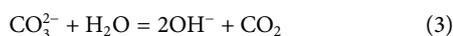
As a result of the heating process, the mineral maturity and hydroxyl substitution percentage increased. This showed that high temperatures not only enhance the crystallinity of HA but also affect the chemical compositions of hydroxyl and carbonate (Ooi et al., 2007). These reactions suggested that the selective loss of type B carbonate ions contributed (at least partially) to the increase in the API during fossilization. Therefore, as mentioned earlier, we present a recommendation of 0.95 as the boundary value of the BC/AC index and 0.10 for the C/P index as preservation indicators of well- and poorly preserved ivory tusks.

The bands at 3,543 cm⁻¹ were observed with different intensities in the spectra at greater than 400℃, while they were practically absent in the spectra of the unheated samples and samples heated below 400℃. Hence, the 3,543 cm⁻¹ band could also be used to characterize the heating history of ivory tusks.

5 Conclusion

FTIR spectra were applied to estimate the preservation state of ancient ivory tusks from the Sanxingdui site. The average SF value of approximately 3.84 for the ancient ivory tusks from the Sanxingdui site was below the threshold of the well-preserved state of bone, indicating a generally well-preserved state. A strong correlation was observed between the API, BPI, and C/P, where the concentrations of the API and BPI decreased approximately linearly as the molar concentration of total carbonate increased in the ivory structure. A BC/AC index value of 0.95 and a C/p value of 0.10 can be used to help identify burnt samples. Thus, the combined evaluation using these indices can contribute to a more efficient evaluation of the preservation state of ancient ivory tusks prior to engaging in expensive and destructive analyses. The *in situ* heating experiments proved that temperature played a role in the preservation results of this study. It can be inferred that the decomposition of the type B carbonate of ancient ivory tusks occurred at over 400℃. The peak position of the structural hydroxyl (3568 cm⁻¹ at 25℃) decreased for the samples heated from 25 to 800℃; however, the 3,543 cm⁻¹ hydroxyl peak was relatively stable, regardless of whether it was newly formed or had already existed. It was clearly verified that an *in situ* high-temperature FTIR spectral analysis can serve as a valuable tool to evaluate the preservation state of ivory tusks.

Data availability statement

The original contributions presented in the study are included in the article/Supplementary Material; further inquiries can be directed to the corresponding authors.

Ethics statement

Ethical review and approval were not required for the animal study because the studied samples were archeological ivory fragments that were unearthed from Sanxingdui ruins.

Author contributions

Formal analysis: XL and CW; funding acquisition: XL and CW; investigation: RZ, YZ, and QX; methodology: XL, RZ, and

WS; supervision: CW; writing—original draft: XL; writing—review and editing: CW, SL, RZ, and QX. All authors have read and agreed to the published version of the manuscript.

Funding

Conflict of interest

The authors declare that the research was conducted in the absence of any commercial or financial relationships that could be construed as a potential conflict of interest.

Publisher's note

All claims expressed in this article are solely those of the authors and do not necessarily represent those of their affiliated organizations, or those of the publisher, the editors, and the reviewers. Any product that may be evaluated in this article, or claim that may be made by its manufacturer, is not guaranteed or endorsed by the publisher.

References

Banerjee, A., Bortolaso, G., and Dindorf, W. (2008). Distinction between african and asian ivory. *Elfenbein Artenschutz* 37.

Bortolaso, G. (2008). Imitations and substitutes for ivory: A short history. *Elfenbein Artenschutz* 27.

Botha, J., Lee–Thorp, J., and Sponheimer, M. (2004). An examination of triassic cynodont tooth enamel chemistry using fourier transform infrared spectroscopy. *Calcif. Tissue Int.* 74 (2), 162–169. doi:10.1007/s00223-003-0124-3

Chi, X. (2013). An explication of the emperor scepter symbol of ancient babylon and ancient China with oraclebone and bronze inscriptions and Relics in Sanxingdui ruins. *Chin. Semiot. Stud.* 9, 126–142. doi:10.1515/css-2013-0110

Edwards, H. G. M., and Farwell, D. W. (1995). Ivory and simulated ivory artefacts: Fourier transform Raman diagnostic study. *Spectrochimica Acta Part A Mol. Biomol. Spectrosc.* 51, 2073–2081. doi:10.1016/0584-8539(95)01455-3

Ellingham, S. T. D., Thompson, T. J. U., and Islam, M. (2016). The effect of soft tissue on temperature estimation from burnt bone using fourier transform infrared spectroscopy. *J. Forensic Sci.* 61, 153–159. doi:10.1111/1556-4029.12855

Farlay, D., Panczer, G., Rey, C., Delmas, P. D., and Boivin, G. (2010). Mineral maturity and crystallinity index are distinct characteristics of bone mineral. *J. Bone Min. Metab.* 28, 433–445. doi:10.1007/s00774-009-0146-7

Featherstone, J., Pearson, S., and LeGeros, R. (1984). An infrared method for quantification of carbonate in carbonated apatites. *Caries Res.* 18, 63–66. doi:10.1159/000260749

Fernandes, R., Sponheimer, M., and Roberts, P. (2022). Toothfir: Presenting a dataset and a preliminary meta-analysis of Fourier Transform Infra-red Spectroscopy indices from archaeological and palaeontological tooth enamel. *Quat. Int.* doi:10.1016/j.quaint.2022.01.010

Flad, R. K. (2012). "Bronze, jade, gold, and ivory: Valuable objects in ancient sichuan," in *The construction of value in the ancient world*. Editors John K. Papadopoulos and Gary Urton (Los Angeles: Cotsen Institute of Archaeology Press), 306–335.

Fleet, M. E. (2009). Infrared spectra of carbonate apatites: ν2-Region bands. *Biomaterials* 30, 1473–1481. doi:10.1016/j.biomaterials.2008.12.007

France, C. A. M., Sugiyama, N., and Aguayo, E. (2020). Establishing a preservation index for bone, dentin, and enamel bioapatite mineral using ATR-FTIR. *J. Archaeol. Sci. Rep.* 33, 102551. doi:10.1016/j.jasrep.2020.102551

Ge, Y., and Linduff, K. M. (2015). Sanxingdui: A new bronze age site in southwest China. *Antiquity* 64, 505–513. doi:10.1017/S0003598X00078406

Gong, W., Yang, S., Zheng, L., Xiao, H., Zheng, J., Wu, B., et al. (2019). Consolidating effect of hydroxyapatite on the ancient ivories from Jinsha ruins site: Surface morphology and mechanical properties study. *J. Cult. Herit.* 35, 116–122. doi:10.1016/j.culher.2018.06.002

Grunenwald, A., Keyser, C., Sautereau, A. M., Crubézy, E., Ludes, B., and Drouet, C. (2014). Revisiting carbonate quantification in apatite (bio)minerals: A validated FTIR methodology. *J. Archaeol. Sci.* 49, 134–141. doi:10.1016/j.jas.2014.05.004

Hammerli, J., Hermann, J., Tollan, P., and Naab, F. (2021). Measuring *in situ* CO2 and H2O in apatite via ATR-FTIR. *Contrib. Mineral. Pet.* 176, 105. doi:10.1007/s00410-021-01858-6

Jantou-Morris, V., Horton, M. A., and McComb, D. W. (2010). The nano-morphological relationships between apatite crystals and collagen fibrils in ivory dentine. *Biomaterials* 31, 5275–5286. doi:10.1016/j.biomaterials.2010.03.025

Krajewski, A., Mazzocchi, M., Buldini, P. L., Ravaglioli, A., Tinti, A., Taddei, P., et al. (2005). Synthesis of carbonated hydroxyapatites: Efficiency of the substitution and critical evaluation of analytical methods. *J. Mol. Struct.* 744-747, 221–228. doi:10.1016/j.molstruc.2004.10.044

Lafon, J.-P., Champion, E., and Bernache-Assollant, D. (2008). Processing of AB-type carbonated hydroxyapatite Ca10− x (PO4) 6− x (CO3) x (OH) 2− x− 2y (CO3) y ceramics with controlled composition. *J. Eur. Ceram. Soc.* 28, 139–147. doi:10.1016/j.jeurceramsoc.2007.06.009

Lai, C. (2015). Archaeological museums and tourism in China: A case study of the Sanxingdui museum. *Mus. Manag. Curatorsh.* 30, 75–93. doi:10.1080/09647775.2015.1008391

Lebon, M., Reiche, I., Bahain, J. J., Chadefaux, C., Moigne, A. M., Fröhlich, F., et al. (2010). New parameters for the characterization of diagenetic alterations and heat-induced changes of fossil bone mineral using Fourier transform infrared spectrometry. *J. Archaeol. Sci.* 37, 2265–2276. doi:10.1016/j.jas.2010.03.024

Lebon, M., Reiche, I., Fröhlich, F., Bahain, J. J., and Falguères, C. (2008). Characterization of archaeological burnt bones: Contribution of a new analytical protocol based on derivative FTIR spectroscopy and curve fitting of the ν1ν3 PO4 domain. *Anal. Bioanal. Chem.* 392, 1479–1488. doi:10.1007/s00216-008-2469-y

Locke, M. (2008). Structure of ivory. *J. Morphol.* 269, 423–450. doi:10.1002/jmor.10585

Madhavasarma, P., Veeraragavan, P., Kumaravel, S., and Sridevi, M. (2020). Studies on physiochemical modifications on biologically important hydroxyapatite materials and their characterization for medical applications. *Biophys. Chem.* 267, 106474. doi:10.1016/j.bpc.2020.106474

Madupalli, H., Pavan, B., and Tecklenburg, M. M. J. (2017). Carbonate substitution in the mineral component of bone: Discriminating the structural changes, simultaneously imposed by carbonate in A and B sites of apatite. *J. Solid State Chem.* 255, 27–35. doi:10.1016/j.jssc.2017.07.025

Mandair, G. S., and Morris, M. D. (2015). Contributions of Raman spectroscopy to the understanding of bone strength. *Bonekey Rep.* 4, 620. doi:10.1038/bonekey.2014.115

Markovic, M., Fowler, B. O., and Tung, M. S. (2004). Preparation and comprehensive characterization of a calcium hydroxyapatite reference material. *J. Res. Natl. Inst. Stand. Technol.* 109, 553–568. doi:10.6028/jres.109.042

Meejoo, S., Maneeprakorn, W., and Winotai, P. (2006). Phase and thermal stability of nanocrystalline hydroxyapatite prepared via microwave heating. *Thermochim. Acta* 447 (1), 115–120. doi:10.1016/j.tca.2006.04.013

Miller, L. M., Vairavamurthy, V., Chance, M. R., Mendelsohn, R., Paschalis, E. P., Betts, F., et al. (2001). *In situ* analysis of mineral content and crystallinity in bone using infrared micro-spectroscopy of the ν4 PO43− vibration. *Biochimica Biophysica Acta - General Subj.* 1527, 11–19. doi:10.1016/S0304-4165(01)00093-9

Müller, K., and Reiche, I. (2011). Differentiation of archaeological ivory and bone materials by micro-PIXE/PIGE with emphasis on two Upper Palaeolithic key sites: Abri Pataud and Isturitz, France. *J. Archaeol. Sci.* 38, 3234–3243. doi:10.1016/j.jas.2011.06.029

Munro, L. E., Longstaffe, F. J., and White, C. D. (2007). Burning and boiling of modern deer bone: Effects on crystallinity and oxygen isotope composition of bioapatite phosphate. *Palaeogeogr. Palaeoclimatol. Palaeoecol.* 249, 90–102. doi:10.1016/j.palaeo.2007.01.011

Ooi, C. Y., Hamdi, M., and Ramesh, S. (2007). Properties of hydroxyapatite produced by annealing of bovine bone. *Ceram. Int.* 33, 1171–1177. doi:10.1016/j.ceramint.2006.04.001

Paris, C., Lecomte, S., and Coupry, C. (2005). ATR-FTIR spectroscopy as a way to identify natural protein-based materials, tortoiseshell and horn, from their protein-based imitation, galalith. *Spectrochimica Acta Part A Mol. Biomol. Spectrosc.* 62, 532–538. doi:10.1016/j.saa.2005.01.023

Pedrosa, M., Curate, F., Batista de Carvalho, L. A. E., Marques, M. P. M., and Ferreira, M. T. (2020). Beyond metrics and morphology: The potential of FTIR-ATR and chemometrics to estimate age-at-death in human bone. *Int. J. Leg. Med.* 134, 1905–1914. doi:10.1007/s00414-020-02310-3

Pekounov, Y., and Petrov, O. E. (2008). Bone resembling apatite by amorphous-to-crystalline transition driven self-organisation. *J. Mat. Sci. Mat. Med.* 19, 753–759. doi:10.1007/s10856-007-3085-7

Roberts, P., Louys, J., Zech, J., Shipton, C., Kealy, S., Carro, S. S., et al. (2020). Isotopic evidence for initial coastal colonization and subsequent diversification in the human occupation of Wallacea. *Nat. Commun.* 11, 2068. doi:10.1038/s41467-020-15969-4

Roche, D., Ségalen, L., Balan, E., and Delattre, S. (2010). Preservation assessment of miocene–pliocene tooth enamel from tugen hills (Kenyan rift valley) through FTIR, chemical and stable-isotope analyses. *J. Archaeol. Sci.* 37, 1690–1699. doi:10.1016/j.jas.2010.01.029

Rujitanapanich, S., Kumpapan, P., and Wanjanoi, P. (2014). Synthesis of hydroxyapatite from oyster shell via precipitation. *Energy Procedia* 56, 112–117. doi:10.1016/j.egypro.2014.07.138

Seredin, P., Goloshchapov, D., Ippolitov, Y., and Vongsvivut, J. (2020). Development of a new approach to diagnosis of the early fluorosis forms by means of FTIR and Raman microspectroscopy. *Sci. Rep.* 10, 20891. doi:10.1038/s41598-020-78078-8

Shaltout, A. A., Allam, M. A., and Moharram, M. A. (2011). FTIR spectroscopic, thermal and XRD characterization of hydroxyapatite from new natural sources. *Spectrochimica Acta Part A Mol. Biomol. Spectrosc.* 83, 56–60. doi:10.1016/j.saa.2011.07.036

Shi, Jingsong (2005). Re-Examination of the artifact pits of Sanxingdui. *Chin. Archaeol.* 5, 200–208. doi:10.1515/CHAR.2005.5.1.200

Snoeck, C., and Pellegrini, M. (2015). Comparing bioapatite carbonate pre-treatments for isotopic measurements: Part 1—impact on structure and chemical composition. *Chem. Geol.* 417, 394–403. doi:10.1016/j.chemgeo.2015.10.004

Sponheimer, M., and Lee-Thorp, J. A. (1999). Alteration of enamel carbonate environments during fossilization. *J. Archaeol. Sci.* 26, 143–150. doi:10.1006/jasc.1998.0293

Surovell, T. A., and Stiner, M. C. (2001). Standardizing infra-red measures of bone mineral crystallinity: An experimental approach. *J. Archaeol. Sci.* 28, 633–642. doi:10.1006/jasc.2000.0633

Tacker, R. C. (2008). Carbonate in igneous and metamorphic fluorapatite: Two type A and two type B substitutions. *Am. Mineral.* 93, 168–176. doi:10.2138/am.2008.2551

Thompson, T. J. U., Gauthier, M., and Islam, M. (2009). The application of a new method of Fourier Transform Infrared Spectroscopy to the analysis of burned bone. *J. Archaeol. Sci.* 36, 910–914. doi:10.1016/j.jas.2008.11.013

Thompson, T. J. U., Islam, M., Piduru, K., and Marcel, A. (2011). An investigation into the internal and external variables acting on crystallinity index using Fourier Transform Infrared Spectroscopy on unaltered and burned bone. *Palaeogeogr. Palaeoclimatol. Palaeoecol.* 299, 168–174. doi:10.1016/j.palaeo.2010.10.044

Tonsuaadu, K., Gross, K. A., Plūduma, L., and Veiderma, M. (2012). A review on the thermal stability of calcium apatites. *J. Therm. Anal. Calorim.* 110 (2), 647–659. doi:10.1007/s10973-011-1877-y

Virág, A. (2012). Histogenesis of the unique morphology of proboscidean ivory. *J. Morphol.* 273, 1406–1423. doi:10.1002/jmor.20069

Weiner, S., and Bar-Yosef, O. (1990). States of preservation of bones from prehistoric sites in the near east: A survey. *J. Archaeol. Sci.* 17, 187–196. doi:10.1016/0305-4403(90)90058-D

Wright, L. E., and Schwarcz, H. P. (1996). Infrared and isotopic evidence for diagenesis of bone apatite at dos pilas, Guatemala: Palaeodietary implications. *J. Archaeol. Sci.* 23, 933–944. doi:10.1006/jasc.1996.0087

Xu, J. J. (2008). *The Sanxingdui site: Art and archaeology, Doctoral dissertation*. Princeton University.

Yan, Y., Ge, W., Wang, Y., Xu, C., Wu, Y., and Cui, T. (2022). Determining the earliest directly dated cremation tombs in neolithic China via multidisciplinary approaches: A case study at laohudun site. *Int. J. Osteoarchaeol.* 32, 1130–1141. doi:10.1002/oa.3139

Yang, S., and Xu, X. (2022). Bronze masks of mysterious Sanxingdui: Oldest record of graves' disease? *J. Endocrinol. Invest.* 45, 1115–1116. doi:10.1007/s40618-021-01643-z

Yoder, C. H., Landes, N. T., Tran, L. K., Smith, A. K., and Pasteris, J. D. (2018). The relative stabilities of A- and B-type carbonate substitution in apatites synthesized in aqueous solution. *Mineral. Mag.* 80, 977–983. doi:10.1180/minmag.2016.080.035

Yoder, C., Pasteris, J., Worcester, K., Schermerhorn, D., Sternlieb, M., Goldenberg, J., et al. (2012). Dehydration and rehydration of carbonated fluor- and hydroxylapatite. *Miner. (Basel).* 2, 100–117. doi:10.3390/min2020100

Zheng, W., Li, X., Lam, N., Wang, X., Sun, Z., Liu, S., et al. (2013). Application of multi-frequency electromagnetic profiling in studying the distribution of bronze in jinsha ruin worship. *Int. J. smart Sens. Intell. Syst.* 6, 733–751. doi:10.21307/ijssis-2017-563